World Journal of Engineering Research
ISSN: 2959-9873
DOI: https://doi.org/10.61784/wjer3006

EFFECT OF FREQUENCY ON LOSSES IN A 77K MINIATURE PNEUMATIC STIRLING CRYOCOOLER

GengChen Liu[1*], AnKuo Zhang[1], Bo Yu[2], YangPing Zeng[2], Shu Wang[2]
[1]Department of Refrigeration and Cryogenic Engineering, Shanghai Ocean University, Shanghai 201306, China.
[2]Cryocooler Development Department, Zhejiang JueXin Microelectronics Co, Ltd, Lishui 323000, Zhejiang, China.
Corresponding Author: GengChen Liu, Email: Gengchen-Liu@qq.com

Abstract: This paper investigates the impact of frequency on the losses within a 77K miniature pneumatic Stirling cryocooler. Low-temperature cryocoolers are essential for providing a low-temperature working environment for high-performance cooled thermal imaging detectors. Stirling cryocoolers can achieve a higher relative Carnot efficiency under low heat load conditions. By establishing a one-dimensional numerical model and analyzing the mechanisms of various internal losses, this study examines the trends of internal energy loss within different components as a function of working frequency, ultimately determining the optimal frequency for the Stirling cryocooler. The results indicate that flow resistance loss, non-ideal heat transfer loss, axial conduction loss, and shuttle loss are the primary loss types in miniature pneumatic Stirling cryocoolers. Experimental testing and analysis confirm the accuracy of the numerical simulation results and demonstrate the performance of the cryocooler at different frequencies. The cryocooler can achieve a cooling capacity of 905 mW@77 K@ 24.2 W_{in} at its optimal operating condition. This study provides a theoretical basis and experimental support for the design and optimization of miniature Stirling cryocoolers.
Keywords: Stirling cryocooler; Frequency; Losses; Effect; Pneumatic; Mid-wave infrared detector

1 INTRODUCTION

Low-temperature cryocoolers play a crucial role in providing a low-temperature working environment for high-performance cooling-type thermal imaging detectors. For lower thermal noise, typical mid-wave infrared cooling detectors need to operate within a low-temperature range of 70-80 K, which allows them to achieve higher temperature sensitivity, greater measurement distance, and higher spatial resolution compared to non-cooling detectors [1–4]. However, cooling detectors have higher costs, larger sizes, and higher power consumption, which sets higher demands for the cryocooler.

Under low heat load conditions, Stirling cryocoolers can achieve a higher relative Carnot efficiency compared to other types of cryocoolers. The widespread application of linear compressors has greatly enhanced the operational lifespan of pneumatic Stirling cryocoolers compared to rotary Stirling cryocoolers, while significantly reducing the overall size and vibration[5–7]. Therefore, miniature pneumatic Stirling cryocoolers, characterized by small size, long life, low vibration, high refrigeration efficiency, and low weight, can meet the current infrared requirements.

For pneumatic Stirling cryocoolers, the compressor and expander can each be regarded as a vibration system. If their natural frequencies are matched, the cryocooler will be in a resonant state, and operating at the resonant frequency allows for the highest cooling capacity with the least electrical work input. Thus, adjusting the cooling performance and the matching relationship between the expander and compressor can be achieved by varying the operating frequency to find the cryocooler's resonant frequency. During the engineering development process, it is necessary to determine the impact of frequency on the internal energy loss distribution and refrigeration performance of the entire machine to ascertain the cryocooler's resonant frequency.

Over several decades, Thales has developed numerous models of Stirling cryocoolers, including linear split types such as the UP708x, UP8xxx, LSF93xx, LSF95xx, and LSF99xx series[8,9]. Consequently, they have initiated improvements to the previously developed LSF93xx and LSF95xx models to extend their service life. Optimization strategies can be approached from two aspects: internal structure and operational parameters. The optimization plan for the LSF9340/50-HA models focuses on operational characteristics, specifically the detailed determination of operating frequency and filling pressure [10]. Ricor, a renowned manufacturer in the field of infrared cryogenics, offers products that are quite representative[11]. The K527S is a short cold finger type miniature linear split Stirling cryocooler[12]. The cold finger has been shortened from the original 44 mm to 19 mm, and the corresponding resonant frequency has increased from 68 Hz to 90 Hz. This indicates that there is an interaction between the structure of the regenerator and the resonance frequency. Cryotech Co, Ltd focuses primarily on the development of low-cost HOT miniature Stirling cryocoolers. The best operating frequency for their split cryocoolers is 80 Hz, with a filling pressure of 1 MPa, and they can achieve a cooling performance of 260 mW@150 K@1.6 W_{ac}[13,14].

From actual manufacturer products, it has been observed that there is a correlation between the structure and materials of the cryocooler and the resonant frequency. Changes in structure and materials will inevitably affect the distribution of internal losses; hence, a connection between losses and resonant frequency is inevitable. Currently, numerous studies involve the analysis of energy flow within the regenerator. From a theoretical standpoint, the cryocooler operates on the inverse cycle of a heat engine, which makes the study of heat engines valuable for the development and optimization of

cryocoolers M.T. Mabrouk et al.[15] derived the energy flow in the gaps of a β-type heat engine, analyzing the impact of gap width on loss conditions. Ruijie Li et al.[16] discussed theoretical or empirical formulas for various losses in Stirling heat engines and optimized the heat engine using the Finite Physical Dimensions Thermodynamics (FPDT) method based on multi-objective criteria. For Stirling heat engines, the GPU-3 modeling approach is widely adopted to study the dynamic characteristics of the engine. Although this method includes the mathematical construction of losses, the focus in engineering is on the entire cycle process and the final cycle efficiency, with less quantitative analysis of losses[17,18]. Swift [19]regarded thermoacoustic theory as a unified perspective for regenerative oscillating heat engines, including cryocoolers. Wang[20,21] elucidated the relationship between electromechanical-acoustics from the perspective of phase coupling. Most studies on cryocoolers are based on empirical formulas and theoretical derivations, using cooling capacity or cooling efficiency as optimization targets to analyze the performance of heat engines or cryocoolers[22]. Therefore, direct attention to the distribution of internal losses within a cryocooler is relatively scarce.
This paper aims to design and develop a 0.5W@77 K miniature split Stirling cryocooler, establishing a one-dimensional numerical model and analyzing the mechanisms of various internal losses. Further research is conducted from the perspective of energy loss to study the impact trends of working frequency on the internal energy loss of different components, ultimately determining the optimal frequency for this Stirling cryocooler.

2 LOSS TYPES IN MINIATURE PNEUMATIC STIRLING CRYOCOOLERS

A higher coefficient of performance (COP) indicates a more efficient and effective refrigerator. The factors affecting COP are the irreversible loss due to the flow resistance of the viscous working medium and the entropy generated by the conduction between the working medium and the wall surface. In general, irreversible loss can be divided into non-ideal heat transfer loss, flow resistance loss, conduction loss and shuttle loss[23]. Therefore, the study of the mechanism of irreversible loss can fundamentally weaken or avoid the loss, which will contribute to the optimization of the refrigerator.

2.1 Non-ideal Heat Transfer Losses

During the operation of a cryocooler, the flowing gas undergoes heat exchange with the original cavity gas, the heat sink wire mesh, and the walls. However, due to imperfect thermal dynamics, complete and effective heat exchange often cannot be achieved, leading to energy loss known as non-ideal heat transfer losses [24]. The majority of these losses occur within the regenerator.
The performance of a regenerator is typically assessed by its heat exchange efficiency, which can be simply represented as the ratio of actual heat transfer to the ideal heat transfer under specified design and operating conditions. As one of the key components in a Stirling cryocooler, the quality of the regenerator's performance dictates the ultimate performance of the cryocooler. The regenerator, being a type of heat exchanger, can have its efficiency defined using the number of transfer units (NTU)[25]:

$$\varepsilon = \frac{NTU}{NTU + 2} \tag{1}$$

$$NTU = \frac{A_{wetted} h}{\dot{m}_{ave,r} C_p} \tag{2}$$

where A_{wetted} represents the wetted surface area involved in heat transfer within the regenerator, $\dot{m}_{ave,r}$ represents the average mass flow rate through the regenerator, C_p represents the specific heat capacity at constant pressure of the working gas, and h represents the heat transfer coefficient, given by the equation[26],

$$h = \frac{Nu\lambda_g}{D_r} = \frac{\lambda_g}{D_r} C_1 (\mathrm{Re}_{ave} Pr)^{C_2} \tag{3}$$

In the equation, λ_g represents the thermal conductivity of the working gas, C_1 and C_2 are the empirical coefficients ($C_1 = 0.42$, $C_2 = 0.67$), D_r represents the diameter of the regenerator, and Re_{ave} represents the average Reynolds number, Pr represents the Prandtl number.

Therefore, the non-ideal heat transfer loss ($\dot{Q}_r$) is defined as:

$$\dot{Q}_r = \dot{m}_{ave,r} C_p (1 - \varepsilon) (T_H - T_C) \tag{4}$$

where T_H and T_C are the temperatures at the hot end and the cold end, respectively.
In practical applications, the regenerator is often designed with a matrix of wire mesh or porous material that provides a large surface area for heat transfer while allowing the working gas to flow through with minimal resistance. The choice of material, its porosity, and the geometric configuration are critical factors that influence the regenerator's ability to facilitate heat exchange without excessive energy loss.

2.2 Flow Resistance Losses

The working gas in a Stirling cryocooler passes through the regenerator and various pipes, and due to its own viscosity and the roughness of the walls, it generates flow resistance, leading to a decrease in pressure amplitude and thus a loss of cooling capacity. This type of loss is referred to as flow resistance loss. The flow resistance loss is caused by the reduction of expansion work in the cold space due to gas pressure drop, and the average flow resistance loss can be defined as the reduced expansion work [23,27]. And the formula is as follows:

$$\dot{Q}_{ave,fr} = \frac{1}{t}\int_0^t \Delta p_r(t)\,dV(t) \tag{5}$$

$$\Delta p_r(t) = \Delta p_{r,\max}\cos(\omega t) \tag{6}$$

$$\Delta p_{r,\max} = \frac{f_r \rho l_r U^2}{2D_r} \tag{7}$$

In the formula, t represents a running cycle, f_r represents the Fanning friction coefficient, ρ represents the gas density, U represents the axial gas flow velocity amplitude.

According to the experimental testing by Gedeon and Wood [28], the Fanning friction factor is related to the Reynolds number, , and the following formula exists:

$$f_r = 129\,\mathrm{Re}^{-1} + 2.91\,\mathrm{Re}^{-0.103} \tag{8}$$

2.3 Shuttle Losses

The displacer in a Stirling cryocooler plays a crucial role in exchanging the working gas between the compression space and the expansion space, while also maintaining a relatively constant temperature difference between the two working spaces. As the displacer moves towards the hot end from the center of its stroke, its surface temperature is lower than that of the cylinder wall at the same axial position. Consequently, heat is transferred from the cylinder to the displacer. Similarly, as the displacer moves towards the cold end, its surface temperature is higher, transferring heat from the displacer to the cylinder. Due to the thermal capacity of the displacer's surface, the temperature oscillation of the displacer is out of phase with its motion[29,30]. At a certain axial position, the enthalpy flow accompanying the displacer's motion in the cold direction is always greater than that in the hot direction. The net enthalpy flow rate from the hot region to the cold region is referred to as the shuttle heat, resulting in shuttle heat loss, which can be calculated using the following formula [31]:

$$\dot{Q}_{shuttle} = \frac{\pi D_r S}{4} 2\pi f \lambda \rho c T_{10} \tag{9}$$

$$T_{10} = \Gamma S \frac{a_2}{\sqrt{\left(\frac{a_1+a_2}{\sqrt{2}}\right)^2 + \left(\frac{a_1+a_2}{\sqrt{2}} + a_1 a_2\right)^2}} \tag{10}$$

In the formula, S represents the stroke of the displacer, f represents the operating frequency, c represents the specific heat capacity, Γ represents the temperature gradient,. The dimensionless numbers a_1 and a_2 are defined based on the characteristics of the space, heat transfer coefficient, and frequency, with the specific expression being:

$$a_1 = \frac{k_1}{h'}\sqrt{\frac{2\pi f}{\alpha_1}} \tag{11}$$

$$a_2 = \frac{k_2}{h'}\sqrt{\frac{2\pi f}{\alpha_2}} \tag{12}$$

where h' represents the heat transfer coefficient, k_1 and k_2 respectively represent the thermal conductivity of the displacer and cylinder, α_1 and α_2 respectively represent the thermal diffusivity of the displacer and cylinder.

2.4 Pumping Losses

In Stirling cryocoolers, the pressure within the working space varies cyclically, leading to the presence of gas in the clearance between the displacer and the cylinder wall that either originates from or flows into the expansion space. This gas can absorb and transfer energy from the surrounding walls. Specifically, when the system pressure increases, the gas pressure within the clearance is lower than that in the expansion space, allowing a small amount of cold gas to enter the clearance from the expansion space and absorb heat from the displacer and cylinder walls, as well as from the initially present gas within the clearance[32]. Conversely, when the system pressure decreases, the gas pressure within the clearance becomes higher than in the expansion space, causing the gas to flow back into the expansion space. Due to non-ideal heat transfer between the gas and the displacer and cylinder walls, the temperature of the gas flowing into the

expansion space is higher than the space's temperature, resulting in heat release to the expansion space and an increased heat load at the cold end. This leads to a loss of cooling capacity for the cryocooler, known as pump gas loss[33,34]. The pump gas loss can be estimated using the following formula [35]:

$$\dot{Q}_{pump} = 4.04\,(T_H - T_C)\,\delta^{2.6}\left[\frac{fC_p}{RT_{ave}}\left(\frac{p_{\max}}{Z_H} - \frac{p_{\min}}{Z_C}\right)\right]^{1.6}\left(\frac{\pi D_r}{\lambda_g}\right)^{0.6} \tag{13}$$

2.5 Heat Conduction Losses

In a Stirling cryocooler, a significant temperature difference exists between compression space and the expansion space. Although they are separated by a regenerator, heat conduction cannot be ignored. The axial heat conduction losses through the regenerator matrix, cylinder walls, and wire mesh represent an additional thermal load on the regenerator. This loss is independent of the frequency and pressure of the refrigerator, and can be calculated according to Fourier's law of thermal conductivity [36,37], the specific formula is:

$$\dot{Q}_{cond,i} = k_i \frac{A_i}{l_i}(T_H - T_L) \tag{14}$$

In the given formula, k_i represents the thermal conductivity of different components (regenerator shell, cylinder, wire mesh), A_i represents the axial heat conduction cross-sectional area of different components, and l_i represents the axial length of different components.

This loss is crucial to consider in the design and optimization of Stirling cryocoolers, as it impacts the overall efficiency and cooling performance of the system. Minimizing these conduction losses is essential for achieving higher coefficients of performance and better refrigeration capabilities, especially in applications requiring cryogenic temperatures for infrared detectors, superconducting magnets, and other sensitive instruments

3 NUMERICAL SIMULATION OF INTERNAL LOSSES IN MINIATURE PNEUMATIC STIRLING CRYOCOOLERS

As shown in Figure 1, a miniature pneumatic Stirling cryocooler can be divided into seven parts based on thermodynamic characteristics: the compression space, the secondary compression space, the compressor back pressure space, the expander back pressure space, the expansion space, the connecting tube, and the regenerator. Each of these parts needs to be discretized into many small and uniform sub-regions. These sub-regions can exchange heat, work, and mass with their surroundings through their own boundaries, and the entire process can be described by a set of differential equations. Based on the nodal analysis of the miniature pneumatic Stirling cryocooler and specific design parameters (as shown in Table 1), a one-dimensional model of the cryocooler is constructed using SAGE software.

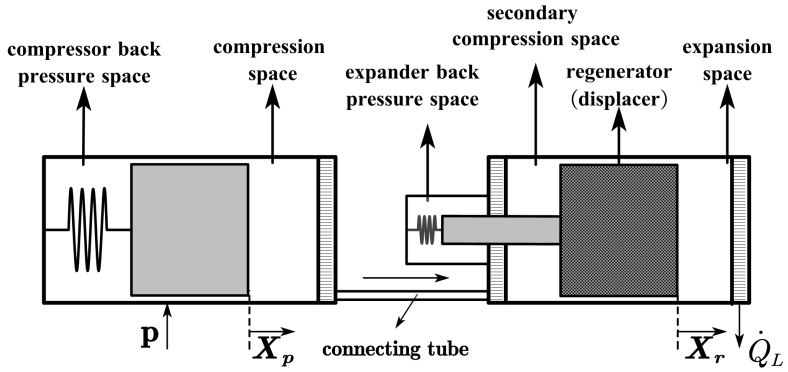

Figure 1 Simplified Model of Miniature Pneumatic Stirling Cryocooler[38]

Table 1 Partial Design Parameters of Miniature Pneumatic Stirling Cryocooler

	Name	Parameter Values
Target Parameters	cooling capacity	≥0.5 W
	refrigeration temperature	77 K
Operating Parameters	pressure	2.0 MPa
	frequency	80-120 Hz
	input power	≤25 W
Parts	compression space	Volume 0.302 cm^3
	compressor back pressure space	Volume 1.563 cm^3
	secondary compression space	Volume 0.068 cm^3
	regenerator	Outer diameter 7.6 mm Inner diameter 7.5 mm

	Length 38.6 mm
	400# Stainless steel wire mesh
expansion space	Volume 0.091 cm^3
expander back pressure space	Volume 0.628 cm^3

3.1 Internal Loss Distribution of Miniature Pneumatic Stirling Cryocooler

Figure 2 illustrates the distribution of internal energy losses in a split Stirling cryocooler. Among the four types of losses, the largest is due to flow resistance, accounting for 40% of the total losses, followed by non-ideal heat transfer losses at 35.6%, while conduction losses at 21.9% and shuttle losses at 2.5% are comparatively smaller. Concurrently, it is observed that the regenerator contributes the highest losses, constituting 50% of the total losses.
Secondly, irreversible losses generated in the connecting tubes can reach one-fifth of the total losses. Other components of the cryocooler produce irreversible losses below 10%, particularly within the working spaces, with the back pressure cavities of both components having negligible impact. In particular, the pumping loss, essentially an additional energy loss due to inadequate heat exchange between the gas and the walls within the clearance, can be attributed to the non-ideal heat transfer loss within the clearance and thus is not discussed separately.

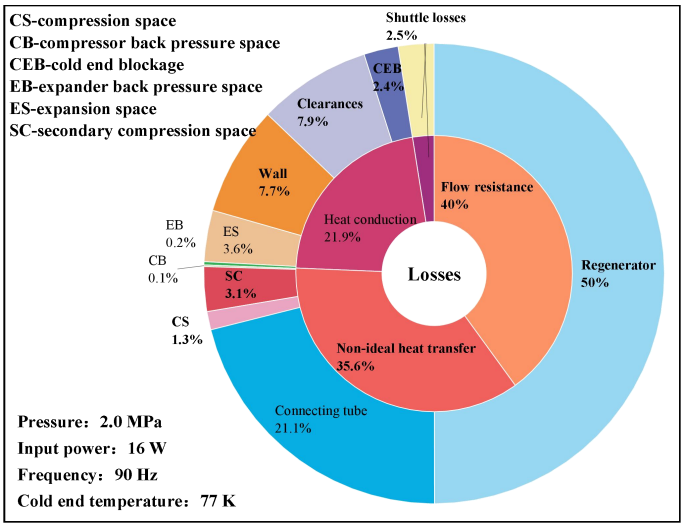

Figure 2 Internal Loss Distribution Chart of Miniature Pneumatic Stirling Cryocooler

Figure 3 presents the variation curves of the three dominant losses, total losses, and cooling capacity with respect to frequency, demonstrating the significant influence of operating frequency on cooling performance and internal losses. As the frequency increases from 80 Hz to 110 Hz, the cooling capacity rises from 0.79 W to 087 W and then decreases to 0.62 W, peaking at 90 Hz. The trend of total flow resistance losses is opposite to that of the cooling capacity, achieving a minimum value at a frequency of 94 Hz. Meanwhile, the total axial conduction losses increase with frequency, but the trend for total non-ideal heat transfer losses is contrary.

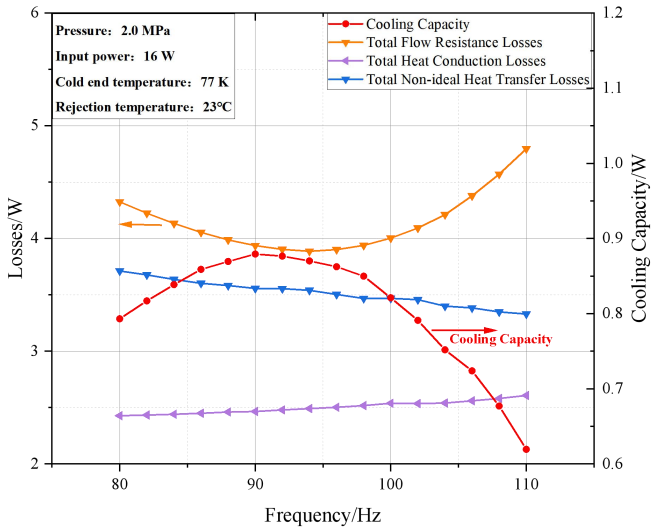

Figure 3 The curve of total internal loss and cooling capacity of the refrigeration machine varying with frequency.

3.2 The Impact of Frequency on Internal Losses in the Regenerator

During the operation of the cryocooler, the internal conditions of the regenerator often deviate from the ideal state, leading to energy loss. The regenerator's heat exchange matrix, composed of a wire mesh, directly engages in heat exchange with the reciprocating working fluid. However, the thermal capacity of the metal mesh is not infinitely large as assumed in ideal conditions, which prevents the mesh from fully storing the heat from the gas or transferring all stored cold energy to the working fluid. This characteristic of non-ideal heat transfer results in entropy generation. Moreover, the wire mesh packed within the regenerator forms a non-uniform porous medium that partially impedes the flow of the working fluid. The viscous nature of the working fluid causes a reduction in pressure amplitude as it passes through the packing, leading to flow resistance losses. Additionally, axial conduction through the heat exchange matrix also contributes to certain conduction losses.

As depicted in Figure 4, while maintaining a constant filling pressure of 2.0 MPa, the pressure drop loss within the regenerator varies from 3.20 W to 2.39 W as the operating frequency is adjusted from 80 Hz to 110 Hz, reaching a minimum at 104 Hz. With the increase in operating frequency, the number of heat exchange occurrences between the working fluid and the heat exchange matrix per unit time correspondingly increases [39], leading to a reduction in non-ideal heat transfer loss from 1.95 W to 1.58 W. The maximum variation in axial conduction loss of the matrix is 20 mW. The total internal loss within the regenerator, which is the sum of the aforementioned three types of losses, gradually decreases with frequency and achieves a minimum at 108 Hz. The results indicate that moderately increasing the operating frequency can effectively reduce Non-ideal heat transfer losses, and there exists an optimal frequency that minimizes pressure drop losses. However, the axial loss of the heat exchange matrix does not exhibit significant variation with frequency changes.

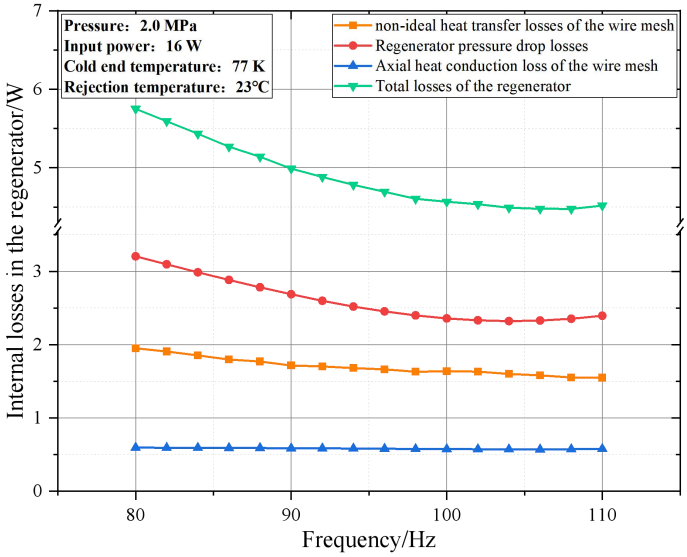

Figure 4 The Curve of Internal Losses in the Regenerator Varying with Frequency

3.3 The Impact of Frequency on Internal Losses within the Connecting Tube

The interconnecting tube between the compressor and the expander is directly exposed to the external environment, allowing the working fluid passing through the thin walls to engage in heat exchange with the surroundings, leading to a substantial loss of energy through heat dissipation. Moreover, due to the small diameter and considerable length of the connecting tube, when the working fluid transitions from a larger volume space into the slender tube, the local and frictional resistances cause a reduction in pressure amplitude[40]. Figure 5 illustrates the variation curves of the pressure drop within the connecting tube, as well as the flow resistance and non-ideal heat transfer losses as a function of operating frequency. Notably, the pressure drop across the connecting tube increases rapidly with the rise in operating frequency, resulting in an increase in flow resistance loss from 0.85 W to 1.271 W, following a similar trend to the pressure drop. However, the increase in the number of heat exchange occurrences compensates for the non-ideal heat transfer; as the frequency rises from 80 Hz to 110 Hz, the heat exchange loss is reduced by 0.5 W. Nevertheless, since the pressure drop loss predominates within the connecting tube, the total loss exhibits an overall increasing trend with frequency.

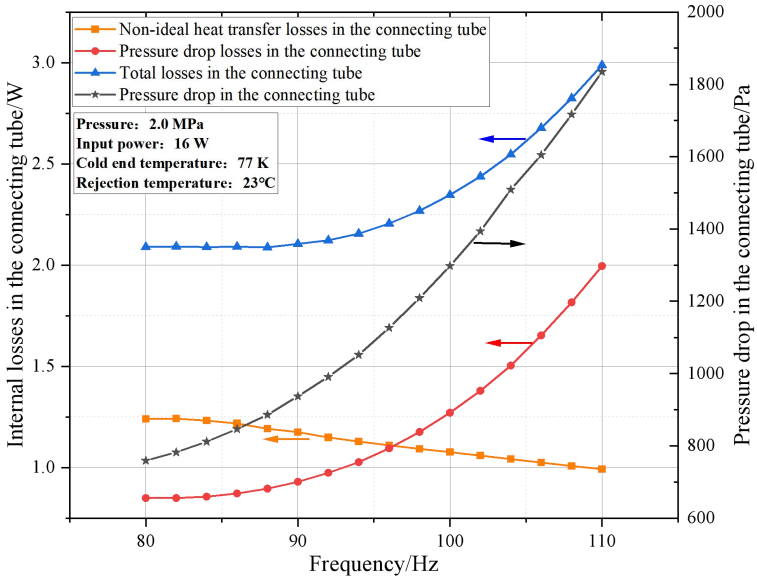

Figure 5 The Curve of Internal Losses and Pressure Drop in the Connecting Tube Varying with Frequency

3.4 The Impact of Frequency on Losses in Clearances of Various Components

Clearance sealing, as one of the key technologies of linear Stirling cryocoolers, draws attention to the energy losses within the clearances. The most significant clearance losses are concentrated in the space between the regenerator and the cold finger wall. The fixed clearance volume between the displacer and the cylinder wall facilitates gas lubrication between the displacer and the cold finger wall; however, due to the viscous nature of the gas, frictional losses are inevitable. Additionally, since there are temperature gradients both axially and radially within the gap, heat exchange between the gap gas and the walls on either side, as well as with the cold end gas, is unavoidable. This alters the temperature of a portion of the heat in the regenerator and the expansion space gas to some extent, resulting in additional thermal loading.

Figure 6 illustrates the relationship between losses within various clearances and frequency variation. The total loss within the regenerator gap (the sum of shuttle loss and regenerator gap loss) significantly exceeds the clearance losses between the step shaft (displacer) and the compressor. As the frequency increases from 80 Hz to 110 Hz, losses in each gap tend to increase, indicating that a higher frequency leads to greater gap leakage. The shuttle loss fluctuates around 0.25 W and, since it depends on the operational characteristics of the regenerator and the temperature difference between the cold and hot ends, the displacer's travel will follow a similar pattern of change.

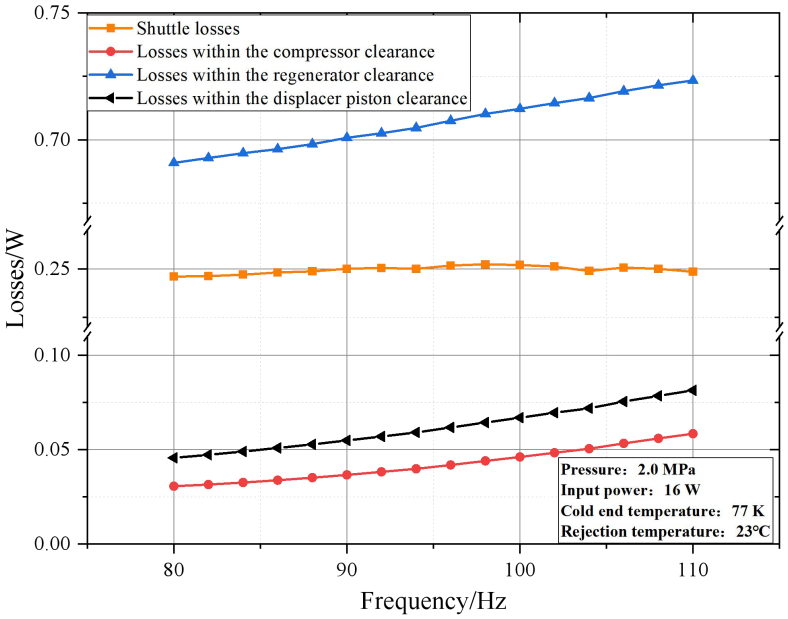

Figure 6 The Curve of Internal Losses in the Clearances of Various Components Varying with Frequency

4 EXPERIMENTAL TESTING AND ANALYSIS

According to the simulation results, a miniature split Stirling cryocooler was designed and manufactured, followed by preliminary testing. It should be noted that the cryocooler was placed inside a temperature-controlled chamber, where the environmental temperature was regulated by adjusting the internal temperature of the chamber. The heat balance method was employed to test the cooling capacity. A heating element and temperature sensors were coupled inside the dewar, and once thermal equilibrium was achieved inside the dewar, the heating power value was numerically equal to the cooling capacity at the corresponding cold end temperature. Figure 7 presents the cooling curve under specific conditions, showing that under a certain heat load, the cold end temperature was reduced from 296 K to 77 K in 3.75 minutes, demonstrating the potential for rapid cooling of the Stirling cryocooler.

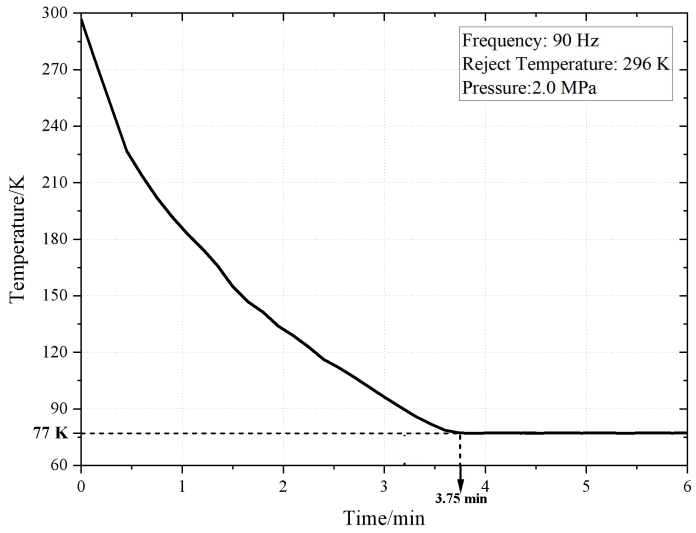

Figure 7 The Cooling Curve of Miniature Stirling Cryocooler

Figure 8 illustrates the distribution of the cryocooler's cooling efficiency and compressor efficiency at different frequencies, as well as the cooling performance at the optimal frequency. Figure 8(a) further indicates that under an input power of 9 W, the COP distribution aligns with the simulated predicted trend, increasing with frequency and peaking at 90 Hz for optimal efficiency. The compressor efficiency varies with frequency in a similar manner to the cooling efficiency, but the frequencies corresponding to their peak efficiencies differ by 2 Hz. The compressor efficiency of around 80% suggests a suitable match between the compressor and the expander. Figure 8(b) presents the cryocooler's performance under high-temperature and room-temperature conditions. At a room temperature of 23℃, the cryocooler can achieve a cooling capacity of 905 mW@77 K@ 24.2 W_{in}. Notably, the cooling performance under high-temperature conditions is inferior to that under room temperature but still meets the demand for a cooling capacity of 500 mW. Under high temperatures, the regenerator cannot exchange heat with the surroundings as effectively as at lower temperatures, leading to a buildup of heat at the hot end and a reduction in cooling efficiency. Therefore, increasing heat exchange fins to enhance heat transfer is a simple yet effective extrinsic solution.

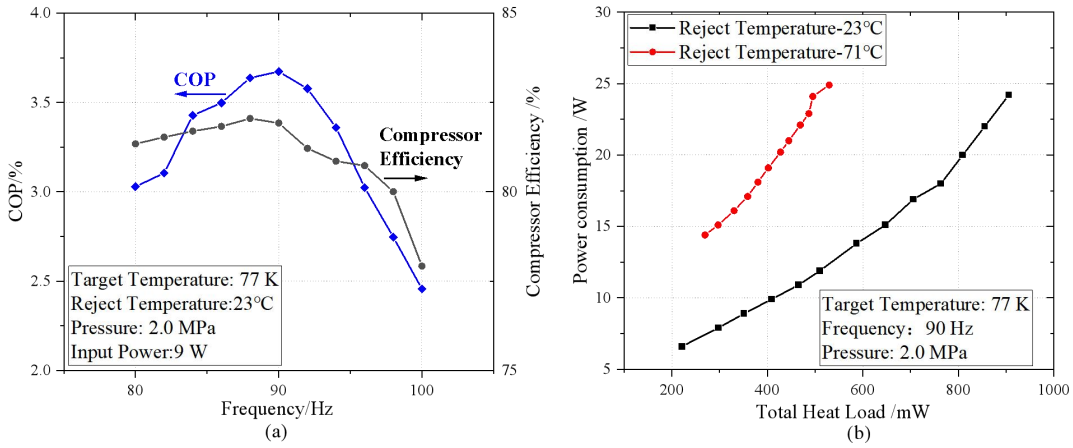

Figure 8 The Actual Performance of the Miniature Stirling Cryocooler: (a) The Distribution of Cop and Compressor Efficiency with Frequency, (b) The Cooling Performance under High-Temperature and Room-Temperature Conditions

5 CONCLUSION

Through a detailed analysis of the internal losses in a 77K miniature pneumatic Stirling cryocooler, this study identifies

key factors affecting the cooling performance. Numerical simulation and experimental testing reveal that flow resistance loss is the most significant component of total losses, with non-ideal heat transfer loss and axial conduction loss also having a notable impact on cooling performance. The study further demonstrates that operating frequency significantly influences the distribution of internal energy losses and the cooling performance of the cryocooler. By adjusting the operating frequency, the resonant frequency of the cryocooler can be identified, thereby achieving optimal cooling performance. Experimental results validate the accuracy of the numerical model and show that the cryocooler achieves peak cooling performance at a frequency of 90 Hz. Additionally, the experiments indicate that the cooling performance of the cryocooler declines in high-temperature environments but can be improved by increasing heat exchange fins to enhance heat transfer efficiency. This research provides important theoretical guidance and experimental data support for the design, optimization, and application of miniature Stirling cryocoolers.

COMPETING INTERESTS

The authors have no relevant financial or non-financial interests to disclose.

REFERENCES

[1] Zhang Y, Wang X, Huang S, et al. Performance of a Highly Integrated Micro Linear Stirling Cooler with Active Vibration Cancellation. IOP Conference Series: Materials Science and Engineering, 2024: 130143. DOI: https://doi.org/10.1088/1757-899X/1301/1/012143.

[2] Xi Z, Zhang X, Jiang H. Heat-dynamics network model and energy analysis of a miniature free piston Stirling cryocooler for application of high operating temperature infrared detector. International Journal of Refrigeration, 2024. DOI: https://doi.org/10.1016/j.ijrefrig.2024.08.014.

[3] Han Y, Zhang A. Cryogenic technology for infrared detection in space. Scientific Reports, 2022, 12: 2349. DOI: https://doi.org/10.1038/s41598-022-06216-5.

[4] Willems D, Arts R, Buist J, et al. Synergies between designed-for-space and tactical cryocooler developments, ICC, 2018.

[5] Sun J, Zeng Y, Huang T, et al. A 150 K Micro Linear Split Stirling Cryocooler for High Operating Temperature Infrared Detectors. International Cryogenic Engineering Conference and International Cryogenic Materials Conference, Springer, 2022: 724–31. DOI: https://doi.org/10.1007/978-981-99-6128-3_94.

[6] Nussberger M, Zehner S, Withopf A, et al. Update on AIM HOT cooler developments. Infrared Technology and Applications XLV, 2019, 11002: 54-62. DOI: https://doi.org/10.1117/12.2520488.

[7] Yun L, Wei H, Wenfan Y, et al. HOT linear cooler developments at KIP. Third International Computing Imaging Conference (CITA 2023), 2023, 12921: 427–36. DOI: https://doi.org/10.1117/12.2688444.

[8] Arts R, Martin JY, Willems D, et al. Miniature cryocooler developments for high operating temperatures at Thales Cryogenics. SPIE Defense + Security, 2015. DOI: https://doi.org/10.1117/12.2176323.

[9] Arts R, Martin JY, Willems D, et al. Miniature Stirling cryocoolers at Thales Cryogenics: qualification results and integration solutions. SPIE Defense + Security, 2016. DOI: https://doi.org/10.1117/12.2228681.

[10] Willems D, Veer BD, Arts R, et al. High-availability single-stage Stirling coolers with high power density. IOP Conference Series Materials Science and Engineering, 2020, 755: 012044. DOI: https://doi.org/10.1088/1757-899X/755/1/012044.

[11] Filis A, Carmiel M, Nachman I. Ricor's advanced rotary and linear miniature cryocoolers for HOT IR detectors. Defense + Commercial Sensing, 2022.

[12] Veprik A, Vilenchik H, Riabzev S, et al. Microminiature linear split Stirling cryogenic cooler for portable infrared imagers. Infrared Technology and Applications XXXIII, 2007, 6542: 823–34. DOI: https://doi.org/10.1117/12.715622.

[13] Veprik A, Gedeon D, Radebaugh R, et al. Low-cost cryogenic technologies for high-operating temperature infrared imaging. Infrared Technology and Applications XLIX, 2023, 12534: 60–77. DOI: https://doi.org/10.1117/12.2664389.

[14] Veprik A, Refaeli R, Wise A, et al. Disruptive cryocoolers for commercial IR imaging. Infrared Technology and Applications XLVIII, 2022, 12107: 120–32. DOI: https://doi.org/10.1117/12.2618257.

[15] Mabrouk MT, Kheiri A, Feidt M. Effect of leakage losses on the performance of a β type Stirling engine. Energy, 2015, 88:111–7. DOI: https://doi.org/10.1016/j.energy.2015.05.075.

[16] Li R, Grosu L, Queiros-Conde D. Multi-objective optimization of Stirling engine using Finite Physical Dimensions Thermodynamics (FPDT) method. Energy Conversion and Management, 2016, 124: 517–27. DOI: https://doi.org/10.1016/j.enconman.2016.07.047.

[17] Hachem H, Gheith R, Aloui F, et al. Technological challenges and optimization efforts of the Stirling machine: A review. Energy Conversion and Management, 2018, 171: 1365–87. DOI: https://doi.org/10.1016/j.enconman.2018.06.042.

[18] Parlak N, Wagner A, Elsner M, et al. Thermodynamic analysis of a gamma type Stirling engine in non-ideal adiabatic conditions. Renewable Energy, 2009, 34: 266–73. DOI: https://doi.org/10.1016/j.renene.2008.02.030.

[19] Swift GW. Thermoacoustics: A unifying perspective for some engines and refrigerators. Springer, 2017.

[20] Wang B, Guo Y, Chao Y, et al. Acoustic-Mechanical-Electrical (AcME) coupling between the linear compressor and the Stirling-type cryocoolers. International Journal of Refrigeration, 2019, 100: 175–83. DOI: https://doi.org/10.1016/j.ijrefrig.2019.01.023.
[21] Bo W, Yijun C, Haoren W, et al. A miniature Stirling cryocooler operating above 100 Hz down to liquid nitrogen temperature. Applied Thermal Engineering, 2021, 186: 116524. DOI: https://doi.org/10.1016/j.applthermaleng.2020.116524.
[22] Getie MZ, Lanzetta F, Bégot S, et al. Reversed regenerative Stirling cycle machine for refrigeration application: A review. International Journal of Refrigeration, 2020, 118: 173–87. DOI: https://doi.org/10.1016/j.ijrefrig.2020.06.007.
[23] Ahmadi MH, Ahmadi M-A, Pourfayaz F. Thermal models for analysis of performance of Stirling engine: A review. Renewable and Sustainable Energy Reviews, 2017, 68: 168–84. DOI: https://doi.org/10.1016/j.rser.2016.09.033.
[24] Hachem H, Gheith R, Aloui F, et al. Optimization of an air-filled Beta type Stirling refrigerator. International Journal of Refrigeration, 2017, 76: 296–312. DOI: https://doi.org/10.1016/j.ijrefrig.2017.02.019.
[25] Li R, Grosu L. Parameter effect analysis for a Stirling cryocooler. International Journal of Refrigeration, 2017, 80:92–105. DOI: https://doi.org/10.1016/j.ijrefrig.2017.05.006.
[26] Tanaka M, Yamashita I, Chisaka F. Flow and heat transfer characteristics of the Stirling engine regenerator in an oscillating flow. JSME International Journal Ser 2, Fluids Engineering, Heat Transfer, Power, Combustion, Thermophysical Properties, 1990, 33: 283–9. DOI: https://doi.org/10.1299/jsmeb1988.33.2_283.
[27] Rohsenow WM, Hartnett JP, Ganic EN. Handbook of heat transfer fundamentals, 1985.
[28] Gedeon D, Wood JG. Oscillating-flow regenerator test rig: hardware and theory with derived correlations for screens and felts. 1996.
[29] Li R, Grosu L, Queiros-Conde D. Multi-objective optimization of Stirling engine using Finite Physical Dimensions Thermodynamics (FPDT) method. Energy Conversion and Management, 2016, 124: 517–27. https://doi.org/10.1016/j.enconman.2016.07.047.
[30] Pfeiffer J, Kuehl H-D. Optimization of the appendix gap Design in Stirling Engines. Journal of Thermophysics and Heat Transfer, 2016, 30: 831–42. DOI: https://doi.org/10.2514/1.T4729.
[31] Segado MA, Brisson JG. Appendix Gap Losses with Pressure-Driven Mass Flows. ICC, 2012.
[32] Strauss JM, Dobson RT. Evaluation of a second order simulation for Sterling engine design and optimisation. Journal of Energy in Southern Africa, 2010, 21: 17–29.
[33] Shendage D, Kedare S, Bapat S. Cyclic analysis and optimization of design parameters for Beta-configuration Stirling engine using rhombic drive. Applied Thermal Engineering, 2017, 124: 595–615. DOI: https://doi.org/10.1016/j.applthermaleng.2017.06.075.
[34] Mahmoodi M, Pirkandi J, Alipour A. Numerical simulation of beta type stirling engine considering heat and power losses. Iranian Journal of Mechanical Engineering Transactions of the ISME, 2014, 15: 5–27. DOI: https://doi.org/20.1001.1.16059727.2014.15.2.1.4.
[35] Cun-Quan Z, Yi-Nong W, Guo-Lin J, et al. Dynamic simulation of one-stage Oxford split-Stirling cryocooler and comparison with experiment. Cryogenics, 2002, 42: 577–85. DOI: https://doi.org/10.1016/S0011-2275(02)00098-X.
[36] Timoumi Y, Tlili I, Nasrallah SB. Design and performance optimization of GPU-3 Stirling engines. Energy, 2008, 33: 1100–14. DOI: https://doi.org/10.1016/j.energy.2008.02.005.
[37] Getie MZ. Numerical modeling and optimization of a regenerative Stirling refrigerating machine for moderate cooling applications. PhD Thesis. Université Bourgogne Franche-Comté, 2021.
[38] Waele ATAM de, Liang W. Basic dynamics of split Stirling refrigerators. Cryogenics, 2008, 48: 417–25. DOI: https://doi.org/10.1016/j.cryogenics.2008.04.004.
[39] Srinivasan KV, Manimaran A, Arulprakasajothi M, et al. Design and development of porous regenerator for Stirling cryocooler using additive manufacturing. Thermal Science and Engineering Progress, 2019, 11: 195–203. https://doi.org/10.1016/j.tsep.2019.03.013.
[40] Liu S, Jiang Z, Ding L, et al. Impact of operating parameters on 80 K pulse tube cryocoolers for space applications. International Journal of Refrigeration, 2019, 99: 226–33. DOI: https://doi.org/10.1016/j.ijrefrig.2018.12.026.